Novel version of the Fibonacci superlattices formed of the graphene nanoribbons: transmission spectra

A.M. Korol' [1,2], S.I. Litvynchuk [2]

[1] Laboratory on Quantum Theory in Linkoping, ISIR, P.O. Box 8017, S-580, Linkoping, Sweden
[2] National University for Food Technologies, Volodymyrska str., 68, Kyiv 01601, Ukraine

Keywords graphene, Fibonacci superlattice, nanoribbons, energy spectra.

E-mail: korolam@ukr.net

The energy spectra of the novel version of the graphene-based Fibonacci superlattices (SL) are calculated. The new quasiperiodical factor is considered. The SL is built of the graphene nanoribbons (GNR) and the quasi-periodicity is formed due to the fact that different ribbons are used as individual elements of the SL and are placed along the lattice growth axis in accordance with the Fibonacci inflation rule. In one case, the SL is composed of the smooth-edges and the metal-like armchair NR and we propose to use the metal-like and the semiconductor armchair NR for another case. It is shown that: 1) the difference in values of the quantized transverse quasi-momentum of electrons for different NR is fully enough to form an effective quasi-periodic modulation in the given structure (no additional factors are needed), and the range of the ribbon widths for this purpose is determined; 2) it is important that this range is suitable for practice. We analyze also the dependence of the energy spectra of the studied structure on the geometric parameters of the superlattice as well as on the external electrostatic potential. Attention is drawn, in particular, that in each Fibonacci generation there is the Dirac superlattice gap. Varying the nanoribbons width one can change the spectra investigated flexibly. The conductance of the structure studied is also calculated. The results obtained can be useful in determining the optimum parameters of devices of the graphene-based nanoelectronics.

1 Introduction In recent years, much attention has been paid to the study of graphene and various graphene-based structures. This is due to non-trivial properties of graphene, such as a linear dispersion law for the quasi-particles, whose behavior at low energies is described by an equation similar to the Dirac-Weyl one, unusual quantum Hall effect, the property of chirality, the Klein tunneling, high mobility, ballistic transport, unusual quality in the superconducting state (in particular, the presence of specular Andreev reflection) etc. [16]. It should also be borne in mind that graphene is a promising material in modern electronics in terms of replacing the silicon technology, the development of which has reached its limit for the graphene one. One of the priority directions is to study the various possibilities of regulation of the energy spectrum of the graphene-based structures. To achieve of this goal one can use, in particular, the graphene nanoribbons (see. e.g. [7-8]). Interest in the study of graphene nanoribbons is connected primarily with the fact that they can be used to form an energy gap; there is no such gap in the pristine graphene, and its presence is essential for performing of the graphene-based structures as a transistor-type devices.

At the same time it is known that the semiconductor superlattices (SL) are widely used in order to regulate the energy spectrum (see e.g. [8]). The literature widely reported the study of graphene SL of different types: strictly periodic, disordered, lattices with defects, etc. [14-27]. The quasi-periodic structures, such as the Fibonacci, the Tew-Morse chains and others, occupy a special place among the graphene structures. This is due to their unusual properties, such as the self-similarity, the Cantor nature of the energy spectrum et al. (see e.g. [9-13]). Spectra of graphene superlattices are characterized, in particular, by the presence of a number of forbidden bands among which is the so-called Dirac superlattice gap having a certain original properties [16-17].

In this paper, we study the energy spectra of the graphene nanoribbons that (spectra) are formed under the influence of quasi-periodic factor. Three kinds of nanoribbons are taken into consideration: the metal-like and semiconductor armchair ribbon and the so called smooth-edges one. To create the quasiperiodic modulation we use the metal-like armchair (element *a*) and the smooth-edges ribbons (element *b*) as the elements for one type of the SL and the metal-like armchair (element *a*) and the semiconductor ribbons (element *b*) for another type.

It is shown that the quasi-periodic arrangement of the above combination of ribbons as the various elements of the superlattice can be used as the quasi-periodic factor. We focused at the Fibonacci superlattices since they are the most studied, classical quasi-periodic structure, to which most of the works on the quasi-periodic themes are

devoted. Since the purpose of this work is to identify the main features of the energy spectra of the Fibonacci superlattices, built on the basis of armchair-graphene nanoribbons, we carry out the evaluations in a relatively simple model – not accounting for the presence of defects, boundaries, more precise dispersion law, the interaction of electrons, etc.

2 Model and formulae Consider the graphene superlattice composed of the two different elements of *a* and *b*, which are arranged along the 0*x* axis in the direction of the SL chain. Elements of *a* and *b* are made of graphene nanoribbons of such width (linear dimension along the axis 0*y*) L_m, L_s, L_{sm} which provides the formation of metal-like (*m*), semiconductor (*s*) and smooth-edges (*sm*) nanoribbons. The external electrostatic potential of value of U_a and U_b can be supplied to the elements *a* and *b* respectively.

Superlattice is constructed according to the Fibonacci inflation rule: $a \to b$, $b \to ab$, so that, for example, for the fourth generation, we have: $R_4 = abaab$. We consider two cases: in one of these, the areas with attached thereto nonzero potentials U_a and U_b (potential barriers) are directly adjacent to one another, and in another case, the quantum wells (that is areas with the fixed zero potential $U = 0$) of width *w*, are placed between the barriers. As will be seen, the spectra of these two kinds of SL have some significant differences.

The wave functions of the quasiparticles in the structure under consideration can be found from the masless Dirac-Weyl equation:

$$[v_F(\boldsymbol{\sigma},\mathbf{p})+U(x)\hat{\mathrm{I}}]\Psi=E\Psi, \qquad (1)$$

where v_F is the Fermi velocity, $\mathbf{p} = (p_x, p_y)$ the momentum operator, $\boldsymbol{\sigma} = (\sigma_x, \sigma_y)$, σ_x, σ_y the Pauli matrices for the pseudospin. Let us enumerate the different areas of the SL by the symbol j ($j = 1,2,3 \ldots$) and assume that the electrostatic potential inside each barrier is constant, that is, we consider the rectangular barriers. Taking into account the translational invariance of solutions relative to the axis 0*y* and presenting it as a sum of plane waves moving in forward and backward directions along the axis 0*x*, the solution of equation (1) for the structure under consideration can be written as

$$\Psi_n(x) = \left[a_{jn} e^{iq_{jn}x} \begin{pmatrix} 1 \\ g^{+}_{jn} \end{pmatrix} + b_{jn} e^{-iq_{jn}x} \begin{pmatrix} 1 \\ g^{-}_{jn} \end{pmatrix} \right], \qquad (2)$$

(in this and subsequent formulae units $\hbar = v_F = 1$ are adopted), top line refers to the graphene sublattice *A*, lower - to *B*, the index *n* is the mode number that corresponds to the size quantized transverse quasi-momentum k_{nj}, quasi-electrons dispersion law has the form

$$E = U_j + \sqrt{q_j^2 + k_{jn}^2}\,, \qquad (3)$$

quantities $g^{\pm}_{j;n}$ equal:

$$g^{\pm}_{j;n} = \frac{\pm q_j + ik_{nj}}{E}\,. \qquad (4)$$

For the smooth-edges ribbons

$$k_{n;sm} = \frac{\left(n+\frac{1}{2}\right)\pi}{L_{sm}},$$

for the metal-like GSL, *n* – integer,

$$k_{n;m} = \frac{n\pi}{L_m}, \qquad (5)$$

for the semiconducting one

$$k_{n;s} = \frac{\left(n+\frac{1}{3}\right)\pi}{L_s}\,. \qquad (6)$$

A significant difference in the values of the quasi-momentum for the nanoribbons considered (for primary modes) suggests that this difference can provide the effective quasi-periodic modulation in the system. (But note that the calculations performed show that the difference in values of *k* for the armchair semiconductor and the smooth-edges ribbons is insufficient for this purpose).

The coefficient of the transmission of the quasi-electrons through the lattice T_n can be found with the help of the transfer matrices method, using the technique of the mode matching of the eigenfunctions at the barrier-well boundaries. Energy range for which $T_n \approx 1$, forms the allowed bands, and gaps correspond to the values of $T_n << 1$. As this procedure is well covered in the literature (see. e.g. [15-27]), we can immediately proceed to analyzing the results obtained.

3 Results and discussion Fig. 1 shows the dependence of $\log T_1$ by the fourth generation on energy *E* for the fourth Fibonacci generation for considered SL based on the metal-like and the semiconductor graphene armchair nanoribbons with the parameters: $L_m \approx 36{,}9$ nm, $L_s \approx 35{,}18$ nm, $d_m \approx 16{,}24$ nm, $d_s \approx 15{,}74$ nm, $w \approx 32{,}48$ nm, the external potential is zero, $n = 1$, i.e. this is the spectrum for the first mode (for convenience, the geometrical dimensions are given in nanometers and energy - in electron volts). In the spectrum, there is a clear trend towards grouping of the spectral bands in the individual cells and the whole spectrum reveals a pronounced periodic character. Note that the density of the spectral lines (maxima, for example) in the fixed energy range increases with the width of elements *a* or *b*. The narrowing of gaps is observed with energy increasing, so that the transmission ratio asymptotically approaches to unity. This narrowing, however, is not a monotone one, the "wavy damped oscillation" in Fig.1 is associated with such property of the spectra as their self-similarity (as in e.g. [23]).

So, there are some parts of the spectrum, the structure of which is repeated periodically throughout the energy

scale - each of these fragments of the spectrum can be conventionally considered as its period.

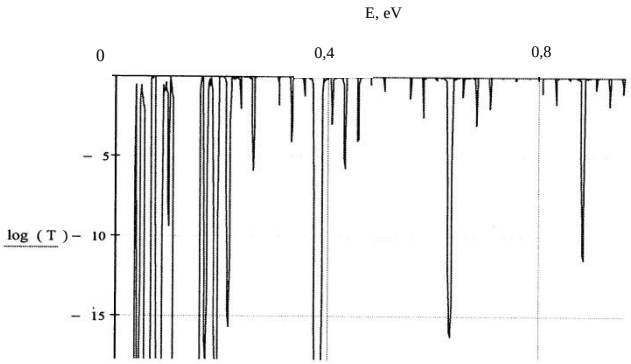

Fig. 1. Dependence of the transmission coefficient T on energy E for the fourth Fibonacci generation.

In the spectrum, it is possible to identify the periods of lesser and greater magnitude and one can select one of these periods for the analysis. Spectra similar to that shown in Fig.1 are implemented for other Fibonacci sequences.

The number of bands in each period, the width of each of them depends greatly on the one hand, the SL parameters, and on the other, the iteration Fibonacci number.

It is well known that the energy spectra in the graphene-based structures can be conveniently controlled by an external electrostatic potential U. We assume that this potential of different magnitude is attached to the SL elements of a: U_a , and to the elements of b: U_b. It is also known that the wide gaps (and the largest number of gaps) is formed in superlattices in the vicinity of the potential barrier ceiling (U). This in particular is confirmed for the structure considered in this paper, as indicated in Fig. 2, which depicts the transmission spectrum for the 4th Fibonacci generation for SL constructed of metal-like and the semiconductor armchair NR with the potential values U_a = 0,4 eV, U_b = 1,6 eV, other parameters: $L_m \approx 36{,}9$ nm, $L_s \approx 35{,}18$ nm, $d_m \approx 16{,}24$, $d_s \approx 15{,}74$ nm, $w = d_m$, $n = 1$. We accepted values U_a и U_b, which differ significantly - in this case two groups of spectral lines are formed around the taken values of the electrostatic potential. When the values of U_a and U_b approach these groups of spectral lines also converge and eventually overlap; in this case the gaps widen.

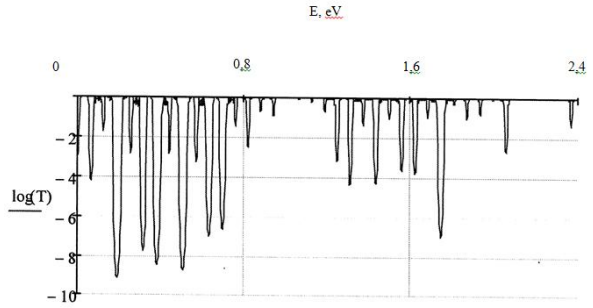

Fig. 2. Dependence of the transmission coefficient T on energy E for the fourth Fibonacci generation for the case of various values of potentials U_m and U_s.

The spectra of higher Fibonacci generations are highly fragmented, also the degree of fragmentation is significantly increased with increase of the geometrical lattice parameters d_s, d_m. With increasing of the Fibonacci sequence the number of gaps increases and their total width grows also.

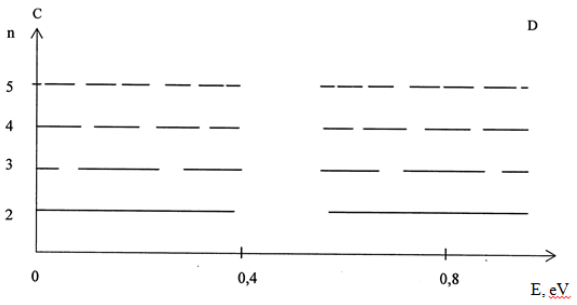

Fig. 3. Trace map for the initial Fibonacci iterations for the SL with the value w=0.

Fig. 3 shows the trace map of the spectra for the SL constructed of the metal-like and the semiconductor armchair NR with w = 0 for the initial Fibonacci generations in the energy period CD for the following parameters: $L_m \approx 29{,}5$ nm, $L_s \approx 24{,}1$ nm, $d_m \approx 16{,}24$ nm, $d_s \approx 15{,}74$ nm, external potential U = 0,5 eV, n = 1.

It can be seen that the spectra have a pronounced fractal nature. The splitting of the allowed bands, starting with the third generation, is in accordance with the property of self-similarity of the Fibonacci spectra. Note that regardless of the values L_s, L_m there are forbidden areas in the spectra for the same energy in all generations. The number of bands in the minimum energy period CD is subjected to the inflationary Fibonacci rule $z_N = z_{N-1} + z_{N-2}$, where z_N - the number of bands in the N-th sequence. For the parame-

ters of Fig. 3, the sequence of numbers z_N, starting with the third generation, is as follows: 6, 8, 14.... . The subordination of the number of bands to the Fibonacci inflation rule is inherent for large periods of the spectra as well, but with its own set of values z_N for each given period.

It is known that the specific Dirac superlattice gap (DSLG) can be formed in the spectrum of graphene superlattices (see e.g. [16-17]). It is of special importance, in particular, due to the fact that it is insensitive to the disorder of geometric lattice parameters [17-18]. The DSLG exists also in the structure considered in this paper and it reveals the additional special property here: the splitting of the allowed bands due to the quasi-periodical factor is the most intensive in the vicinity of this gap, moreover the split bands are located symmetrically with respect to DSLG and the symmetric bands are of equal width. It is clearly seen at Fig. 4 where the trace map for the initial Fibonacci generations is plotted, SL being formed from the smooth-edges and the metal-like nanoribbons, the parameters are as follows: w=0, $L_m \approx$ 36,9 nm, $L_{sm} \approx$ 34,7 nm, $d_m \approx$ 16,24 nm, $d_{sm} \approx$15,1nm, U = 0,6 eV, n = 1.

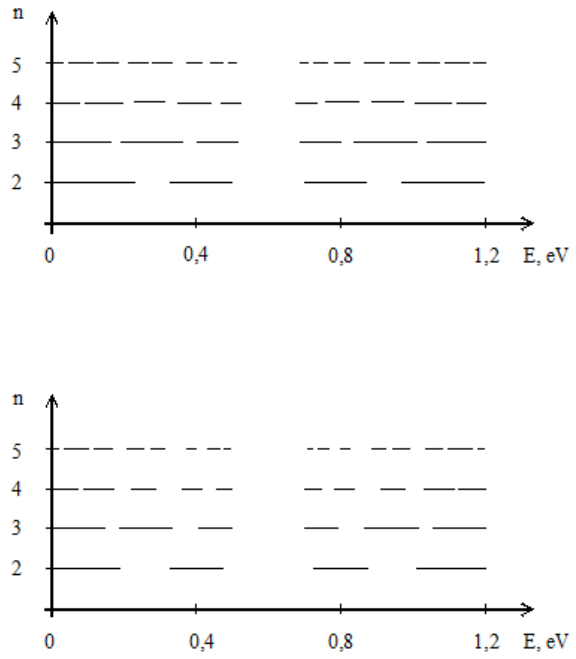

Fig. 4. Trace map for the SL formed of the smooth-edges and the metal-like nanoribbons.

We see that the splitting of bands takes place in accordance with the property of self-similarity. The number of bands in the subsequent generations is subjected to the Fibonacci inflation rule and are equal to 4, 6, 10, 16 in the 2, 3, 4, 5 iterations.

Position of the middle of DSLG can be found using the following equation:

$$cos(k\ell_N) = \frac{1}{2} Tr(M_n), \qquad (7)$$

where k – Bloch quasi-momentum, ℓ_N – lattice period for the N-th Fibonacci generation, M_n – matrix equal to the product of the transfer matrices corresponding to elements of the SL which forms this generation, e.g., for the third generation $M_3 = M_a M_b M_a$. (see e.g. [17]). For an arbitrary Fibonacci generation N, one can obtain for E_{D_N} from the formula (7)

$$E_{D_N} = \frac{U_a \delta_N d_a + U_b d_b}{\delta_N d_a + d_b}, \qquad (8)$$

where $\delta_N = \frac{N_a}{N_b}$, N_a ,N_b the number of relevant elements in this generation. If $U_a \approx U_b = U$, $d_s \approx d_m$ then the value E_{D_N} does not depend on N and equals U. It is obvious that as N increases δ_N tends to a certain constant value and so the value E_{D_N} may significantly depend on the generation number only for the primary sequences, but for higher generations E_{D_N} is practically independent of N. For the parameters of Fig. 3, the value $E_D \approx U$ = 0,5 eV. A characteristic feature of the DSLG is that it is insensitive to the lattice period. This is true for both addressed in this paper types of superlattices: with w=0 and $w \neq 0$. Fig. 5 which shows a spectrum for the fourth Fibonacci generation demonstrates that the Dirac gap remains in place, while others (Bragg ones) shift; the solid line corresponds to the value of the lattice constant (d_m+w) equal to 48,1 nm, dashed – 32,1 nm, values of $L_m \approx$ 36,9 nm, $L_s \approx$ 35,2 nm. SL is formed of the metal-like and the semiconductor armchair ribbons.

The comparison of trace-maps depicted in Fig.3 and Fig.4 for two kinds of SL, namely composed of the metal-like armchair GNR and the smooth-edges ribbons (Fig.4) and metal-like GNR and the semiconductor armchair ribbons (Fig.3), shows that the difference between the values of the transverse quasi-momentum for these two kinds of SL is essential enough for creating the different quasi-periodical energy spectra.

Let us now analyze briefly some features of the spectra of superlattices considered with the fixed quantum wells, that is, those in which between elements a and b (with the applied potentials U_a and U_b respectively), there is a region with the zero potential - the quantum well with a finite width $w \neq 0$. Note that three types of resonances are formed in this type of SL, namely, barrier, "well" and mixed ones [26, 27]. In this case, we should make some corrections to the above results. Thus, the number of gaps increases in the fixed energy range (for example, in the minimal period of the spectrum), besides their number increases substantially with increasing of the quantum well

width. Accordingly, the set of numbers z_N in each period of the spectrum changes. The position of the Dirac band also changes, and in the case of an approximate equality of the quantum well and barrier width the value of $E_D \approx U / 2$. Note that with increasing of the quantum well width the magnitude of the superlattice Dirac gap is reduced, but the adjacent gaps expand.

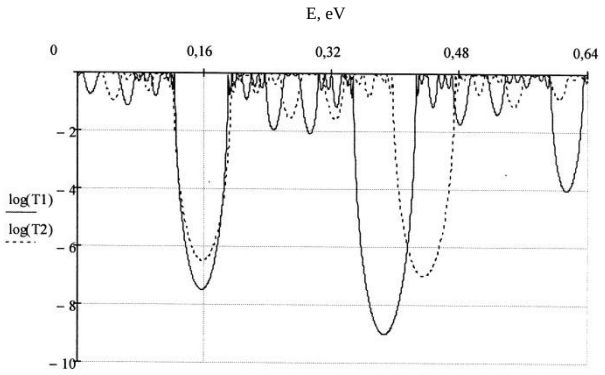

Fig. 5. Transmission spectra for the fourth Fibonacci generation for various magnitudes of the SL period d: values $d_1 \approx$ 48,1nm and $d_2 \approx$ 32,1nm refer to quantities T_1 and T_2 respectively.

Fig. 6 shows the trace map for the SL composed of the metal-like and the semiconductor armchair NR with the following parameters: for figure 6.1 $L_m \approx 36{,}9$ nm, $L_s \approx$ 35,2 nm, for figure 6.2 $L_m \approx 29{,}5$ nm, $L_s \approx 24{,}1$ nm, other parameters for these figures are equal: $d_m \approx 16{,}24$ nm, $d_s \approx 15{,}74$ nm, $w=d_m$, external potential $U = 0{,}5$ eV, $n = 1$. Number of bands in this energy range is subject to Fibonacci inflation rule and for primary sequences is equal to: 2, 3, 5, 8 .... The nature of trace maps in figures 6.1 and 6.2 are the same but the width of allowed (prohibited) bands depends essentially on the values of the nanoribbons width L_m, L_s.

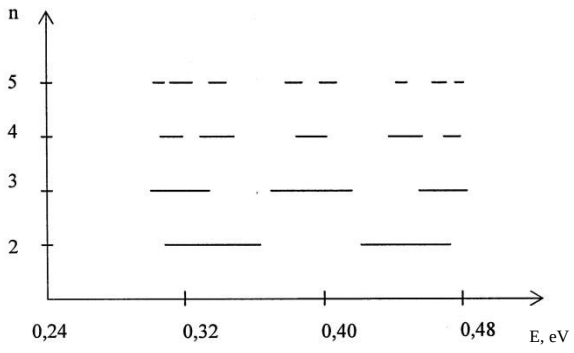

Fig. 6.1.

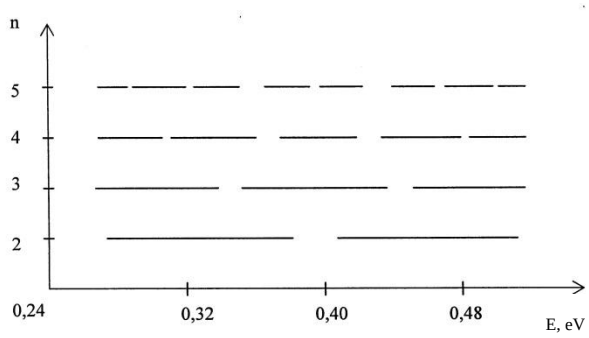

Fig. 6.2. Trace map for the initial Fibonacci generations for the SL ($w \approx d_m$) with various nanoribbon width: for Fig. 6.1 $L_m \approx 36{,}9$ nm; $L_s \approx 35{,}2$ nm; for Fig. 6.2 $L_m \approx 29{,}5$ nm, $L_s \approx 24{,}1$ nm.

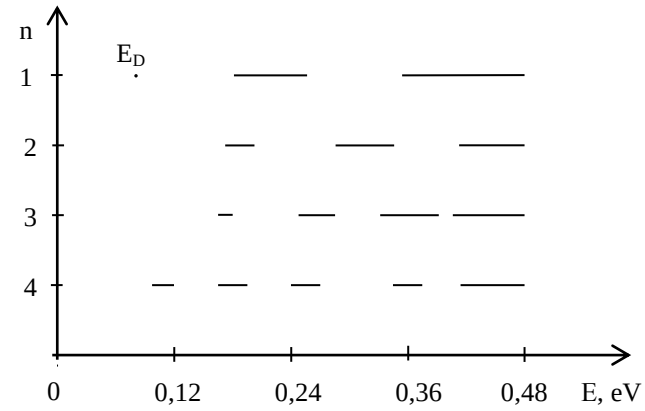

Fig. 7. Trace maps for superlattices with different width of the barriers and the quantum wells (the third Fibonacci sequence).

Fig. 7 presents several trace maps for various values of the parameters of the superlattice formed, as for Fig. 3, of the metal-like and the semiconductor armchair nanoribbons, and this figure illustrates the dependence of the trace maps of the structure considered in this work on the barrier and quantum well width (in the direction of the SL growth, 0x-direction). It is seen that the gaps width, their configuration and the location of bands on energy scale depend significantly on both the barrier and the quantum well width. The trace maps in Fig. 7 refer to the third Fibonacci generation with the following barrier widths: for the first trace map – as in Fig. 3, for the second one – 1.5 and for the third one - 2 times larger than for Fig. 3 (these first three trace maps correspond to the superlattice without the quantum well, i.e. w=0). The potential $U_a=U_b=U$ equals to 0.08 eV. The middle of the Dirac superlattice gap is located at a point $E_D=U$=0.08 eV; we took the energy interval [0, 0.48 eV], so that the trace maps for energies $E>E_D$ are exposed. The gaps widen essentially with the barrier width

increasing; the concentration of gaps in the vicinity of the Dirac SL gap is observed.

The fourth trace map in Fig. 7 refers to the superlattice containing the quantum well of the finite width which is twice lesser than the barrier width for the second trace map in Fig. 7 (still the third Fibonacci sequence is considered). The comparison of the second and the fourth trace maps in Fig. 7 shows, in particular, that the presence of the quantum well changes the configuration of the energy bands significantly; the number of the gaps increases.

Thus the spectra of the structure considered demonstrate the strong dependence on the geometrical parameters of the superlattice as well as on the potential value U. We would like to note that, in general, the spectra investigated are not regular, however we can choose such sets of the parameters involved for which the spectra are regular and may be symmetrical with respect to the Dirac superlattice gap. Note also that the width of the Dirac SL gap depends on the parameters value and it is lesser than the width of some other (Bragg) gaps for various values of the parameters involved.

The conductance of the structures similar to that investigated in this work is known to be often used to analyze the transport properties of such systems – this is the quantity which can be measured in practice. And it is convenient to consider the dimensionless conductance G* (see e.g. [28] and references therein) which can be expressed via the transmission coefficient with the help of the known Landauer formulae (for low temperatures):

$$G^*=\sum_n T_n. \qquad (9)$$

Fig. 8 presents the dependence of the dimensionless conductance G* on energy E for the two types of the superlattice considered: containing a quantum well ($w \neq 0$), Fig. 8.2, and for the SL without a quantum well ($w=0$), Fig. 8.1. The values of the parameters in Fig. 8.2 are the same as for the fourth trace map in Fig. 7; the value of the potential barrier width for Fig. 8.1 is the same as for the second trace map in Fig. 7 and the quantum well width is in 1.5 times lesser. The character of the G* (E) dependence is in general analogous to the transmission rates vs energy dependence. For energies which correspond with the Dirac superlattice gap the conductance has the minimal value: we see the pronounced minimum for energy $E=E_D$ in Fig. 8.1. This value of E_D remains the same with the change of the lattice period $w+d$, but it is very sensitive to the change of the quantity w/d. Thus, varying the SL parameters, in particular, the lattice ones w and d, we can flexibly control the conductance of the system under consideration.

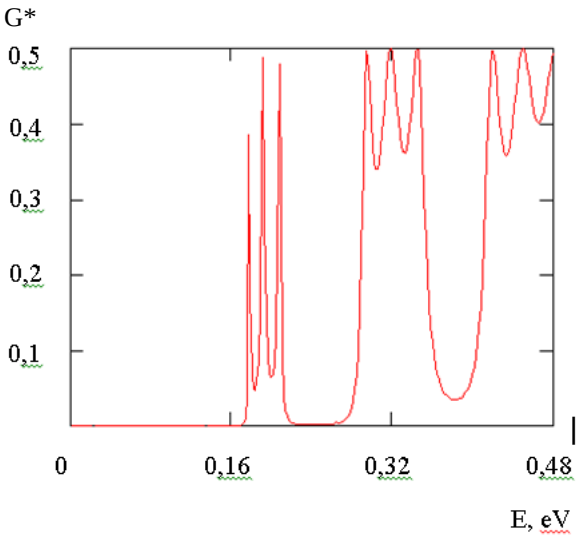

Fig. 8.1. Dependence of the dimensionless conductance G* on energy for the SL without the quantum well (the third Fibonacci sequence).

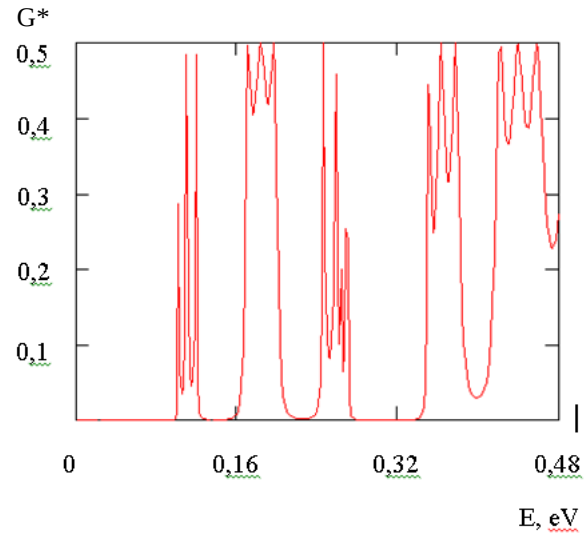

Fig. 8.2. Dependence of the dimensionless conductance on energy for the SL containing the quantum well (the third Fibonacci sequence).

.

4 Conclusion In this paper, we calculate the transmission coefficient of the quasi-electrons through the Fibonacci superlattice built of the graphene armchair metal-like and semiconductor nanoribbons or of the metal-like and the smooth-edges NR; the transmission spectra for the initial Fibonacci generations are presented. These spectra substantially depend on the size of nanoribbons in the direction transverse to the lattice chain direction L. The optimum values of L for the first mode are in the range of several tens of nanometers. The spectra demonstrate the property of periodicity depending on the quasi-electron en-

ergy; bands of the allowed (prohibited) energy values are grouped into individual cells, the structure of which is repeated periodically. The number of energy bands inside each period are subjected to the Fibonacci inflation rule. A spectrum is also significantly dependent on the external electrostatic potential applied to the elements of the SL as well as on the nanoribbons width in the direction of the superlattice growth. In every Fibonacci generation, there is the superlattice Dirac gap the position of which is controlled by the geometric parameters of the lattice, and by the value of the electrostatic potential. The similar energy range (with the same property as the Dirac gap has) is also observed in the conductance vs energy dependence of the structure investigated.

References

[1] A.K. Geim and K.S. Novoselov, *Nat. Materials* **6**, 183 (2007). DOI :10.1038/nmat1849

[2] A.N. Castro Neto, F. Guinea, N.M.R. Peres, K.S. Novoselov, and A.K.Geim, *Rev. Mod. Phys.* **81**,109 (2009). DOI: 10.1103/RevModPhys.81.109

[3] J.M. Pereira, F.M. Peeters, A. Chaves, M. Barbier, and P.Vasilopoulos, *Semicond. Science Technology* **25**,033002 (2010). DOI: 10.1088/0268-1242/25/3/033002

[4] V.V. Cheianov and V.I. Falko, *Phys. Rev. B* **74**, 041403 (2006). DOI: 10.1103/PhyNRevB.74.041403

[5] C.W.J. Beenakker, *Phys.Rev.Lett.* **97**, 067007 (2006). DOI: 10.1103/PhyNRevLett.97.067007

[6] L. Brey and H.A.Fertig, *Phys. Rev. B* **73**, 235411 (2006). DOI: 10.1103/PhyNRevB.73.235411

[7] K. Wakabayashi, K. Sasaki, T. Nakanishi, and T. Enoki, *Sci. Technol. Adv. Mater*. **11**, 054504 (2010). DOI: 10.1088/1468-6996/11/5/054504

[8] R. Tsu. Superlattice to Nanoelectronics (Second edition), Elsevier, Oxford (2011), 327 p.

[9] Z. Cheng, R. Savit, and R. Merlin, *Phys. Rev. B* **37**, 375 (1988). DOI: 10.1103/PhyNRevB.37.375.

[10] E. Macia, *Rep. Prog. Phys.* **75**, 036502 (2012). DOI: 10.1088/0034-4885/75/3/036502

[11] J.M. Luck, *Phys. Rev. B.* **39**, 5834 (1989). DOI: 10.1103/PhysRevB.39.5834

[12] M. Kolar, M.K. Ali, and F. Nori, *Phys. Rev. B.***43**, 1034 (1991). DOI: 10.1103/PhyNRevB.43.1034

[13] N. Liu, *Phys. Rev. B* **55**, 3543 (1997). DOI: 10.1103 / PhyNRevB.55.3543

[14] Q. Zhao, J. Gong, and C.A. Muller, *Phys. Rev. B* **85**, 104201 (2012). DOI: 10.1103/PhyNRevE.90.022921

[15] M. Barbier, P. Vasilopoulos, and F.M.Peeters, *Phil. Trans. R: Soc*. A 386, 5499 (2010). DOI: 1101.4117/Phil.Trans.5499

[16] L. Wang and X. Chen, *J. Appl. Phys.* **109,** 033710 (2011). DOI: 1008. 0504

[17] L. Wang and S. Zhu, *Phys. Rev.B* **81**, 205444 (2010). DOI: 10.1103/PhyNRevB.81.205444

[18] V.H. Nguyen, A. Bournel, and P. Dollfus, *Semicond. Sci. Technol*. **26**, 125012 (2011). DOI: 10.1088/0268-1242/26/12/125012

[19] M. Barbier, P. Vasilopoulos, and F.M. Peeters, *Phys. Rev.B* **80**, 205415 (2009). DOI: 10.1103/PhyNRevB.80.205415

[20] P.Zhao and X.Chen, *Appl. Phys. Lett.* **99**, 182108 (2011).). DOI: 10.1063/1.3658394

[21] T. Ma, C. Liang, L. Wang, and X. Chen, *Appl. Phys. Lett.* **100**, 252401 (2012). DOI. 10.1063/1.4729133

[22] Yu.P.Bliokh, V.Freilikher, S.Savel'ev, and F.Nori, *Phys. Rev. B* **79**, 075123 (2009). DOI: 10.1103/PhyNRevB.79.075123

[23] A.M. Korol and V.M.Isai, Phys. Solid State **55,** 2468 (2013). DOI: 10.1134/S1063783413120147

[24] A.M. Korol, Low Temperature Physics **40**, 324 (2014). DOI: 10.1063/1.4868529

[25] A.M. Korol, V.M.Isai, and N.V. Medvid', Proceedings of the IEEE 34-th International Scientific Conference, Kyiv 2014, P. 235.

[26] P.V. Ratnikov and A.P. Silin, JETP Letters **100**, 349 (2014). DOI: 10.7868/S0370274X14170056

[27] W-Y. Deng, R. Zhu, Y-C. Xiao, and W-J. Deng, *Chin. Phys.* B **23**, 017202 (2014). DOI: 10.1088/1674-1056/23/1/017202

[28] Neetu Agrawal (Garg), Sammer Grover, Sancalpa Ghosh, and Manish Sharma, arXiv:1106.0408v1 [cond-mat.mes-hall] Jun 2011.

Captions to figures

Fig. 1. Dependence of the transmission coefficient T on energy E for the fourth Fibonacci generation.

Fig. 2. Dependence of the transmission coefficient T on energy E for the fourth Fibonacci generation for the case of various values of potentials U_m and U_s.

Fig. 3. Trace map for the initial Fibonacci iterations for the SL with the value w=0.

Fig. 4. Trace map for the SL formed of the smooth-edges and the metal-like nanoribbons.

Fig. 5. Transmission spectra for the fourth Fibonacci generation for various magnitudes of the SL period d: values $d_1 \approx$ 48,1nm and $d_2 \approx$ 32,1nm refer to quantities T_1 and T_2 respectively.

Fig. 6.1, 6.2. Trace map for the initial Fibonacci generations for the SL ($w \approx d_m$) with various nanoribbon width: for Fig. 6.1 $L_m \approx$ 36,9 nm; $L_s \approx$ 35,2 nm; for Fig. 6.2 $L_m \approx$ 29,5 nm, $L_s \approx$ 24,1 nm.

Fig. 7. Trace maps for superlattices with different width of the barriers and the quantum wells (the third Fibonacci sequence).

Fig. 8.1. Dependence of the dimensionless conductance on energy for the SL without the quantum well (the third Fibonacci sequence).
Fig. 8.2. Dependence of the dimensionless conductance on energy for the SL containing the quantum well (the third Fibonacci sequence).